

## ORIGINAL ARTICLE



# Numerical investigation on the fatigue life of non-cracked metallic plates repaired with bonded CFRP

Anis Mohabeddine<sup>(1)</sup>, J.A.F.O. Correia<sup>(1)</sup>, J.M Castro<sup>(1)</sup>, P. Montenegro<sup>(1)</sup>, A.M.P. De Jesus<sup>(2)</sup>, R.A.B. Calçada<sup>(1)</sup>

## Correspondence

Anis Mohabeddine  
Department of Civil Engineering, Faculty of Engineering University of Porto  
Rua Dr. Roberto Frias, s/n 420-465 Porto  
Portugal  
Email: [amohabeddine@fe.up.pt](mailto:amohabeddine@fe.up.pt)

## Affiliations

<sup>1</sup>Department of Civil Engineering, Faculty of Engineering University of Porto (FEUP), Porto, Portugal.

<sup>2</sup>Department of Mechanical Engineering, Faculty of Engineering University of Porto (FEUP), Porto, Portugal

## Abstract

In Europe, a large number of old riveted metallic bridges approach the end of their fatigue life. Past research has shown that the application of CFRP can be very efficient in delaying the crack growth rate of deficient structural elements with existing crack. However, little attention is given to the fatigue resistance of non-damaged metallic members approaching the end of their fatigue life. This is particularly relevant for old metallic riveted bridges, where many critical components do not have existing cracks. This paper presents a numerical investigation on the fatigue behavior of non-cracked metallic plates bonded with CFRP using epoxy resin. Nonlinear finite element analyses are performed using the commercial software ABAQUS. The cyclic elasto-plastic behavior and the fatigue strain life of puddle iron metal are obtained from previous experimental results conducted on specimens extracted from Luiz I Bridge (Porto, Portugal). Debonding failure of the adhesive joint is simulated through the use of cohesive zone model with traction separation law. The cohesive behavior was calibrated using fracture mechanic tests results on the adhesive, conducted in a previous related study. The fatigue crack initiation life was estimated using local approach based on material fatigue strain life. Fatigue resistance curves that relate the number of cycles to failure and the applied nominal stress for unreinforced and reinforced elements are derived. The results show that the application of CFRP can significantly increase the fatigue crack initiation life of a metallic structural component significantly.

## Keywords

Metallic bridge, Puddle iron, Riveted connection, CFRP, fatigue, crack initiation, finite element, cohesive zone model.

## 1 Introduction

The maintenance of aging metallic bridges is a worldwide problem. In Europe, more than 30% of the railway bridge stock is over 100 years old (Wallin *et al.*, [1]). A large portion of these bridges is made of old mild steel or puddle iron, assembled with riveting technology. The nature and the level of loading have changed significantly compared to what they were designed for, a century ago. Old riveted bridges have reached the end of their theoretical design fatigue life.

The replacement of old metallic bridges is economically unfeasible. Therefore, bridge owners usually seek for local repair interventions at components level. The structural elements that are identified to be deficient will be retrofitted to upgrade their performance. Carbon fiber-reinforced polymer (CFRP) is a very attractive material for repairing old metallic structures. The application of CFRP increases the stiffness and strength of the structural elements without modifying their mechanical and fatigue behavior as in it the case of drilling or welding. Besides due to the lightweight of the CFRP laminates, no additional load is added to the structure.

Two decades ago, a benchmark research work on the application of CFRP to extend the fatigue life of metallic bridges was conducted by Bassetti *et al.* [2]–[4] who showed experimental evidence that the application of CFRP to artificially cracked girders and small-scale metallic plates could increase the fatigue life by at least a factor of three. Since then, several experimental studies reported in the technical literature (see refs. [5]–[14]) confirmed the success of the application of CFRP in delaying the fatigue crack growth rate. It was shown that the additional stiffness provided by the CFRP laminates reduces the stress range near the crack tip and crack opening displacement, and also promote the crack closure [4].

Nevertheless, the available studies suggest solutions only for already cracked elements but do not provide any recommendations for delaying or preventing the crack initiation of metallic structural members. However, fatigue crack initiation is very relevant in practical situations since many existing metallic bridge members do not contain cracks, but are rather approaching the end of their design fatigue life (Ghafoori *et al.* [15]–[18]). Hence, research studies on the delaying the crack initiation using bonded CFRP laminates are of paramount interest. Local authorities responsible for the maintenance of old metallic bridges seek to apply the CFRP as preventive measure to extend the fatigue life of non-damaged elements to

avoid crack initiation, rather than repairing already cracked members. For safety reasons, cracked members are usually disassembled and replaced. This process is very complex to apply in situ. The case of old metallic bridges is much more challenging than recent structures because old metallic members can exhibit brittle behavior as in the case of cast-iron. Besides, the material can be incompatible with current steel as in the case of puddle iron. The combination of current steel and puddle iron makes things worse because puddle iron has slightly different electro-potentials that lead to galvanic corrosion. (Harries [19]).

To the knowledge of the authors, only Ghafoori *et al.* [15]–[18] addressed the issue of crack initiation of steel elements reinforced with CFRP. The concept used in the aforementioned studies consisted of estimating the stress concentration using analytical closed form solutions based on elastic theory combined with fatigue stress concentration factor. Then, the fatigue resistance can be identified using the modified Goodman diagram CLD. The authors proposed two design solutions to enhance the fatigue resistance of steel beams by shifting the stresses from risky finite fatigue life to infinite fatigue life in the CLD diagram. The first solution consists of applying pre-stressed CFRP which reduces the mean stress. The second consists of applying non-prestressed ultra-high modulus CFRP to increase the stiffness of the structural element, which will reduce the mean stress and the stress amplitude simultaneously. In *ref.*[17], three steel beams strengthened with non-prestressed CFRP were tested under fatigue loading using the four point loading setup. The results showed that the application of CFRP could extend the fatigue crack initiation life considerably. However, much more experiments are required to address some unknowns related to the fatigue performance of the bonding joint considering different adhesives, different CFRP configurations, and level of loadings.

Within the framework of FIBERBRIDGE “the fatigue strengthening and assessment of railway metallic bridges using fiber-reinforced polymers” research project, the authors recently launched an experimental campaign to investigate the fatigue crack initiation of puddle iron metallic elements reinforced with CFRP plates at the Faculty of Engineering of the University of Porto (FEUP). The puddle iron elements were extracted from an existing bridge (Luiz I Bridge, Portugal) is in service since 1886. Nowadays, this bridge serves the metro (upper deck) and road traffic (lower deck).

This paper presents a numerical study conducted prior to the beginning of the preparation of the specimens of the experimental campaign. The behavior of small-scale specimens made of puddle iron extracted from Luiz I bridge (Porto, Portugal) is simulated in ABAQUS with and without CFRP reinforcements. The constitutive elasto-plastic behavior and the fatigue strain life of the material are obtained from a previous related experimental program De Jesus *et al.* [20]. The bonding behavior between the CFRP and the metallic plates is simulated using cohesive zone modeling that can capture the crack initiation and propagation inside the adhesive layer. Different CFRP configurations are investigated in this study. The non-linear analyses were performed on unreinforced and reinforced models subjected to static loadings with stress higher than the yield strength of the puddle iron. Finally, the fatigue local approach is used to estimate the fatigue resistance of the small-scale metallic elements. The numerical results were correlated with material fatigue strain life to derive fatigue strength curves.

## 2 Geometry and materials

### 2.1 Materials

The mechanical and fatigue behavior of the puddle iron material from the Luiz I Bridge (Proto, Portugal) was comprehensively examined by De Jesus *et al.* [20] and Correia [21]. The mechanical and fatigue properties obtained in the physical tests, which have been reported in the aforementioned studies, constitute the basis of this study for developing the numerical model as well as for the determination of the fatigue resistance of the structural detail.

Previous studies (e.g. Moy, [22]) showed that for civil engineering steel structures, the ultra-high modulus CFRP ( $E > 300GPa$ ) gives the most efficient structural action since it produces a higher elastic modulus than the metal. Therefore, Carbolam® ultra-high modulus CFRP plates are assumed in this numerical study.

The structural adhesive Araldite® AV138 is selected to bond the CFRP plates and the metallic substrate. The choice of the adhesive was motivated by the high strength capacity of the adhesive, see Figure (1), where the tensile strength is higher than 30 MPa, and by the availability of the mechanical and fracture mechanics properties that are provided in Campilho *et al.* [23]. The fracture mechanics properties of the adhesive are essential for the calibration of the cohesive zone model. The basic mechanical properties of the three materials are provided in Table. 1.

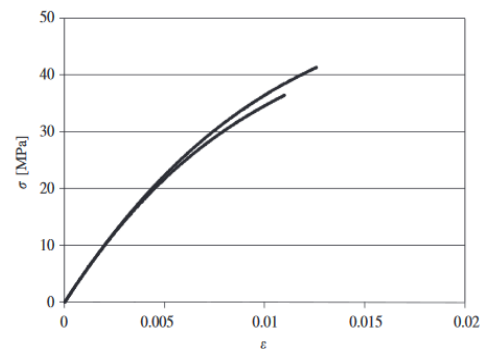


Figure 1: Experimental tensile  $\sigma$ - $\epsilon$  of the adhesive AV138 [23].

### 2.2 Geometrical configurations

This section presents the geometrical properties of the metallic plate used for the numerical simulations, including details of the different CFRP configurations adopted as reinforcements. As shown in Figure (2-a), the metallic plate has a rectangular shape with dimensions of  $140mm \times 75mm$ , and it features a hole in the middle with a diameter  $20mm$ , as typically found in riveted connections in metallic bridges. Figure (2-b) is provided to show the common CFRP patching details used for all other configurations. As can be seen, unidirectional CFRP plates with fibers in the horizontal direction are used. The transversal distance between the CFRP plates and the edge of the hole is taken as  $5mm$ , this distance is left intentionally to consider the area covered by the bolt or the rivet head in practical situations. The length and the width of the CFRP plates used in all configurations are equal to  $130mm$  and  $22.5mm$ , respectively. Figure (3) shows the four CFRP patching configurations considered in this paper. Each specimen is represented by two letters and a numeral, the letters “D-S” stand for double-sided CFRP configuration; “S-S” for single-sided CFRP configuration; and the digits “1” or “2” represent the number of CFRP plates on each side of the specimen. These four patch configurations were considered to cover some practical situations where structural components are not fully accessible in the field. This is particularly relevant for riveted connections, where usually only the outer face of the plate is free to be operated; or sometimes only a partial part of the structural element is accessible.

**Table 1** Tensile mechanical properties of the materials.

Material	Young's modulus E (GPa)	Tensile yield strength $f_y$ (MPa)	Ultimate tensile strength $f_u$ (MPa)	Ultimate tensile strain $\epsilon_u$
Puddle iron <sup>(a)</sup>	192.7	303	397	21%
CFRP <sup>(b)</sup>	440	—	1200	0.27%
Resin <sup>(c)</sup>	4.89	36.49	39.45	1.21%

<sup>(a)</sup> Tested by de Jesus et al. [20]; <sup>(b)</sup> Manufacturer's minimum properties; <sup>(c)</sup> Tested by Campilho et al. [23].

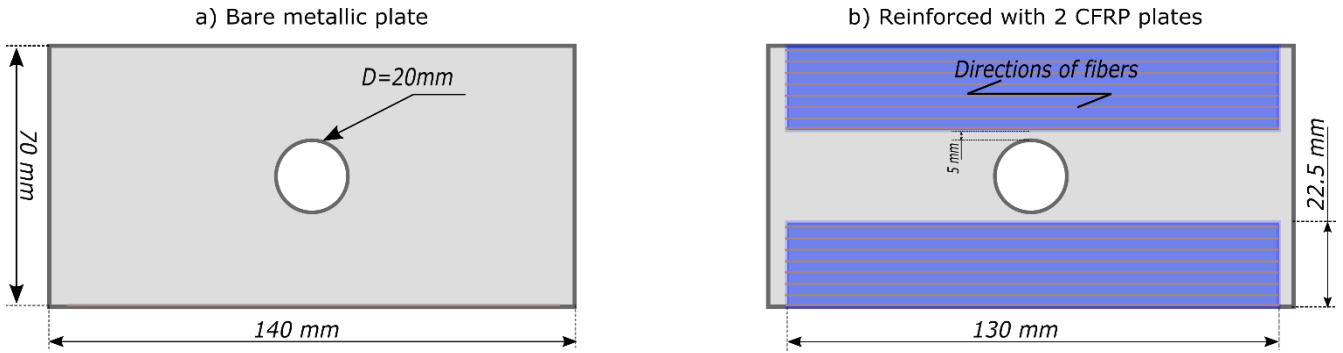


**Figure 2:** Specimens configurations: a) Bare metallic plate; b) Plate reinforced with two CFRP plates.

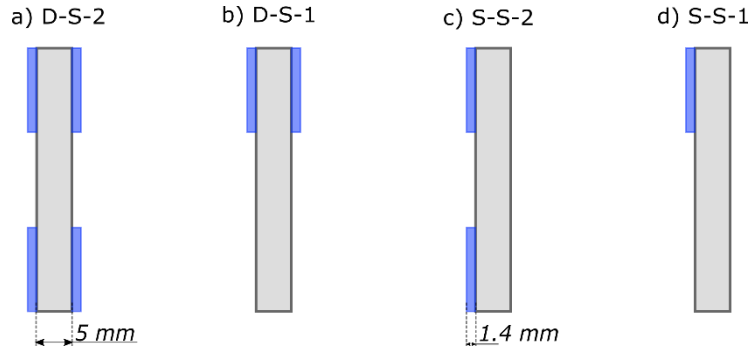


**Figure 3:** Patch configurations: a) Double-sided configuration with 2 CFRP plates on each side; b) Double-sided configuration with 1 CFRP in each side; c) Single-sided configuration with 2 CFRP plates; d) Single-sided configuration with only 1 CFRP plate.



**Figure 4:** Loading and boundary conditions.

### 3 Numerical analysis

#### 3.1 Development of the finite element model

Non-linear finite element analyses were performed in ABAQUS® software. The puddle iron plate was modeled with 8-node three dimensional elements (C3D8R) available in the software's library. The material nonlinearity was considered using the isotropic plasticity model. The engineering stress-strain data provided in ref. [20] was converted to true stress-strain and implemented in the model.

The adhesive layer was modeled using cohesive zone elements (COH3D8) with viscosity  $\eta=1e-4$  and thickness equal to  $1e-4$  mm. More information about the calibration of the cohesive zone elements is provided in the next section.

The CFRP plates were modeled with 3-D continuum shell elements SC8R. The CFRP has a strong unidirectional behavior following the direction of the fibers, and a weaker behavior in the other directions, which is mainly governed by the behavior of the matrix that is usually made of epoxy. Hence, it is more realistic to model the behavior of the CFRP using an orthotropic material model. However, due to the unavailability of experimental data, the CFRP plates were assumed isotropic. This assumption is supported by the study of Haghani [24] who investigated the effect of considering orthotropic or isotropic material models in ABAQUS. His results showed that the isotropic material model gives acceptable results. Besides, verification of the numerical results showed very low level of stress in the direction perpendicular to the fibers. Therefore, the assumption of using isotropic material model is expected to not affect considerably the results.

After a mesh sensitivity study that is not reported herein for brevity, a very refined meshing was adopted in the numerical model, as shown in Figure (5). The mesh size of 1mm was found to be sufficient to provide accurate results for the metallic and CFRP plates. As shown in Figure (5), near the circular hole edge, at stress concentration zone, the mesh size was reduced to 0.5mm. The length of the cohesive zone elements was taken equal to 0.5mm. Smaller mesh rendered the analyses computationally intractable. The previous study conducted by Campilho *et al.* [23] showed that a relatively similar mesh size of the cohesive element (i.e. 0.4mm) provided accurate results compared to experimental data.

In order to allow different meshing between the different parts of the numerical model (i.e. CFRP, cohesive elements, and the metallic plate), each part was meshed separately. Then a pure master-slave contact was used, where the surfaces of the cohesive zone elements are tied to the surfaces of the two adherends. The two surfaces of the cohesive element were considered as the slave surfaces and the others as master surfaces. Figure (4) illustrates the loading and the boundary conditions considered in the numerical model. As can be seen, one edge is fully fixed by restraining in its 6 degrees of freedom. The loading was applied in the horizontal direction at the free edge which was restrained in the vertical direction to avoid undesired distortion near the boundaries. In order to avoid stress concentration near the boundaries, the two edges were constrained as a rigid body with a master reference point where the loading and the BC were assigned. A stepwise static loading protocol was applied with a stress ratio  $R=0$ . The amplitude of loading was equal to 340MPa which is higher than the yield strength of the puddle iron.

#### 3.2 Cohesive zone modeling (CZM)

The cohesive behavior was modeled using the Traction Separation Law (TSL) which is based on the relationship between stresses and

relative displacement of the cohesive element. The TSL simulates the elastic behavior, the damage initiation, and the evolution of damage through a softening behavior until reaching the complete separation of the element. Figure (6) schematically represents these aforementioned steps with its associated nomenclature that will be defined throughout this section.

The elastic constitutive behavior is defined in Equation (1).

$$\sigma = \begin{Bmatrix} t_n \\ t_s \\ t_t \end{Bmatrix} = \begin{bmatrix} K_{nn} & K_{ns} & K_{nt} \\ K_{ns} & K_{ss} & K_{st} \\ K_{nt} & K_{st} & K_{tt} \end{bmatrix} \begin{Bmatrix} \varepsilon_n \\ \varepsilon_s \\ \varepsilon_t \end{Bmatrix} = K \varepsilon \quad (1)$$

The symbols  $t$  and  $\varepsilon$  represent the stress and strain vectors, respectively. The subscripts  $n, s, t$  designate the normal, shear in the principal direction, and shear in the transversal direction, respectively.  $K$  is the penalty stiffness that is determined according to the proposal of Turon *et al.* [25], as shown in Equation (2):

$$K = \alpha \frac{E}{t} \quad (2)$$

where  $E$  is the young's modulus of the adhesive, and  $t$  is the thickness of the adjacent sub-laminate (i.e. CFRP). The parameter  $\alpha$  is a coefficient that should be larger than 1, Turon *et al.* [25] recommended using  $\alpha$  equal to 50.

The Quadratic nominal stress criterion (QUADS), shown in Equation (3) was used to simulate damage initiation.

$$\left\langle \frac{t_n}{t_n^0} \right\rangle^2 + \left\langle \frac{t_s}{t_s^0} \right\rangle^2 + \left\langle \frac{t_t}{t_t^0} \right\rangle^2 = 1 \quad (3)$$

The adhesive strength in each direction is represented by  $t_n^0, t_s^0,$  and  $t_t^0$ . The symbol  $\langle \rangle$  represents the Macaulay brackets that are used to show that a purely compressive stress state does not initiate damage.

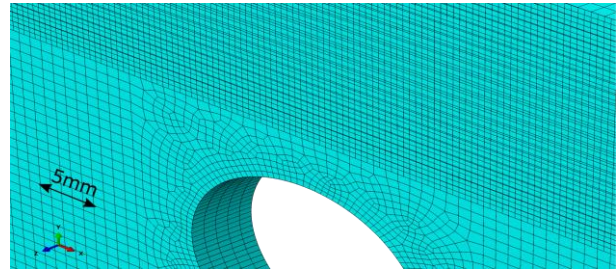


Figure 5: Meshing details: 1mm for the metallic and CFRP plates; 0.5mm near the hole edge; and 0.5 mm for the cohesive zone elements.

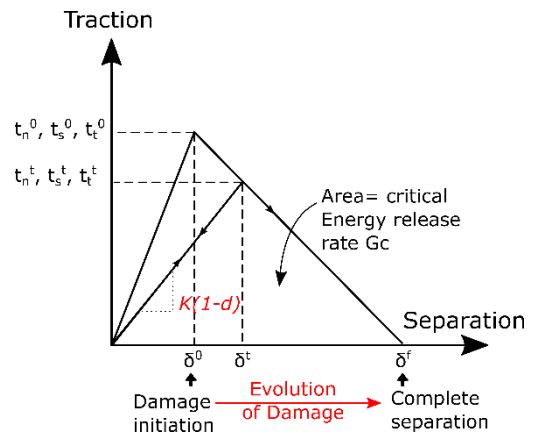


Figure 6: Traction Separation Law (TSL).

Once Equation (3) is satisfied, damage initiates in the cohesive element, which will experience stiffness and strength degradation. This evolution of damage follows the softening curve shown in the TSL curve, see Figure (6). The stiffness degradation is represented in Equation (4), which shows the response of the cohesive element with a damage variable "d", which is equal to 0 when the cohesive element is undamaged and equal to 1 when full failure occurs (Song *et al.* [26]). A linear softening branch is considered for the evolution of damage. This is sufficiently appropriate for brittle adhesives such as Araldite® AV1138 (Campilho *et al.*, [23]).

$$t_i = (1 - d)K_i\Delta_i \tag{4}$$

The complete failure of each element is controlled by the critical fracture energy release rate  $G_c$ . The energy-criterion based on the linear power law is used to predict the complete separation of the cohesive element, as shown in Equation (5).

$$\frac{G_n}{G_n^c} + \frac{G_s}{G_s^c} + \frac{G_t}{G_t^c} = 1 \tag{5}$$

The parameters implemented in the numerical model for cohesive zone modeling are summarized in Table (2).

**Table 2** Parameters of the adhesive for cohesive zone modelling

$K_{nn}$ (N/mm)	174.64	$K_{ss}/K_{tt}$ (N/mm)	174.64
$t_n^0$ (N/mm <sup>2</sup> )	39.45	$t_s^0/t_t^0$ (N/mm <sup>2</sup> )	30.2
$G_n^c$ (N/mm)	0.2	$G_s^c/G_t^c$ (N/mm <sup>2</sup> )	0.38

## 4 Numerical results

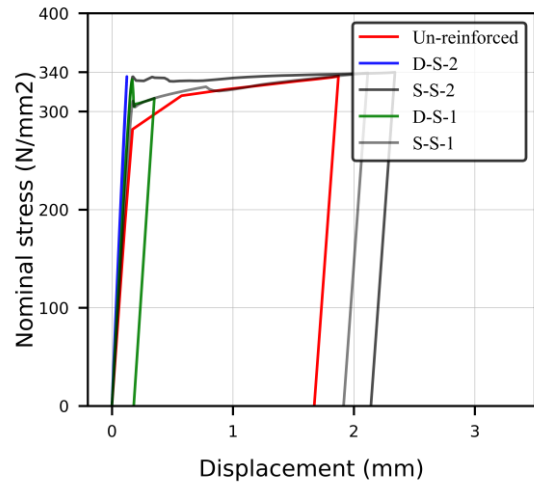
### 4.1 Metallic part

Figure (7) compares the applied nominal stress versus the edge displacement for the unreinforced metallic element and the reinforced elements including the four CFRP configurations. The response of the unreinforced model (shown in red) is presented for comparison. As can be seen, in the first linear branch of Figure (7), the CFRP patches introduced additional stiffness to the metallic elements. Both double-sided CFRP configurations with two and one CFRP plates (i.e. D-S-2 and D-S-1, respectively) reduced significantly the level of displacements. D-S-2 did not experience any non-linear behavior. D-S-1 reached a peak at the maximum applied load, then showed a sudden drop due to partial damage in the cohesive elements. The maximum displacement reached by D-S-1 was equal to 0.35 mm which represents 18% of the total displacement reached in the unreinforced metallic specimen. On the other hand, the models with single-sided CFRP configurations (i.e. S-S-2 and S-S-1) experienced a larger nonlinear displacement than the unreinforced element. This is due to the un-desired bending induced by the non-symmetry of the CFRP plates. This observation have been also observed in physical tests reported by Jones *et al.* [5].

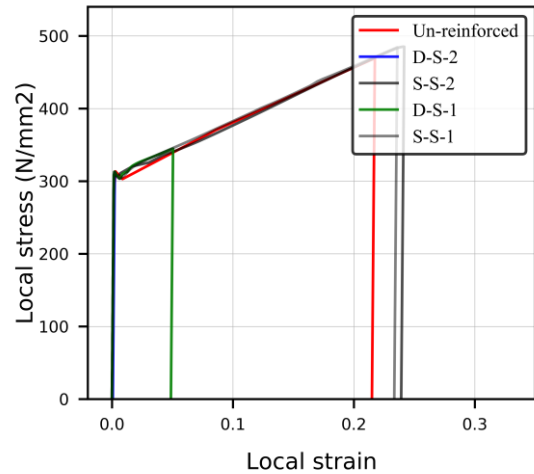
Figure (8) illustrates the local stress-strain curves near the edge of the circular hole, where there is a high level of stress concentration. D-S-2 shows only a linear behavior, whereas D-S-1 experienced some plastic hardening until reaching the stress level of 334Mpa, which is 110% of the yield stress. Models with single-sided configurations (i.e. S-S-2 and S-S-1) experienced large local stress and strain beyond the yield point. Similarly to the global behavior observed in Figure (7), S-S-2 and S-S-1 CFRP configurations experienced higher level of deformations compared to the un-reinforced element.

Figure (9) shows the contour plots of the principal stress in the loading direction for the unreinforced model and the four reinforced

models with CFRP. The stress state in all contour plots is shown at the applied loading of 340MPa nominal stress. The contours are scaled to the yield stress of 303MPa, where beyond it, the color turns to grey.



**Figure 7:** Applied stress versus displacement response of the unreinforced and reinforced metallic elements.



**Figure 8:** Local stress vs. local strain at the stress concentration zone.

Figure (9-a) shows that a large area of the unreinforced model around the central hole has yielded. The maximum level of stress is observed at the circular hole edge with a value of 465MPa. In Figure (9-b), the D-S-2 model shows a clear reduction of stress, where only a small area near the hole has yielded. It can be observed that a high stress level is also present near the edges of the plate. This is mainly due to the abrupt change of stiffness caused by the free gap between the CFRP plate end and the edge of the metallic plate. The value of 365 MPa of local stress is reached at the region between the CFRP and the plate edge. Near the hole, the stress reached only 313MPa which represents 103% of the yield stress. In this study, the focus was only on the stress near the hole, since the stress concentration at the edge of the specimen will depend strongly on the length of the CFRP plate, and in practical situations, the CFRP plates are much longer than 130mm since the designer is required to ensure a minimum anchorage length (Fawzia *et al.*[27]). In Figure (9-c), D-S-1 shows a disproportionate in-plane distribution of stress; higher stresses are present in the bottom part of the plate where there are no CFRP reinforcements. Near the circular hole, the maximum stress reached the value of 344MPa which represents 113% of the

yield stress. Figure (9-d) and Figure (9-e) depict the stress distribution on the back face (i.e. unreinforced side) of one-sided models namely S-S-2 and S-S-1. As stated previously, these two configurations experienced bending stresses due to the asymmetry of the

CFRP plates. Therefore, the level of maximum stress in these models reached higher values than in the unreinforced model. The maximum stress reached in S-S-2 and S-S-1 was observed at the hole edge with values of 490MPa and 485MPa, respectively.

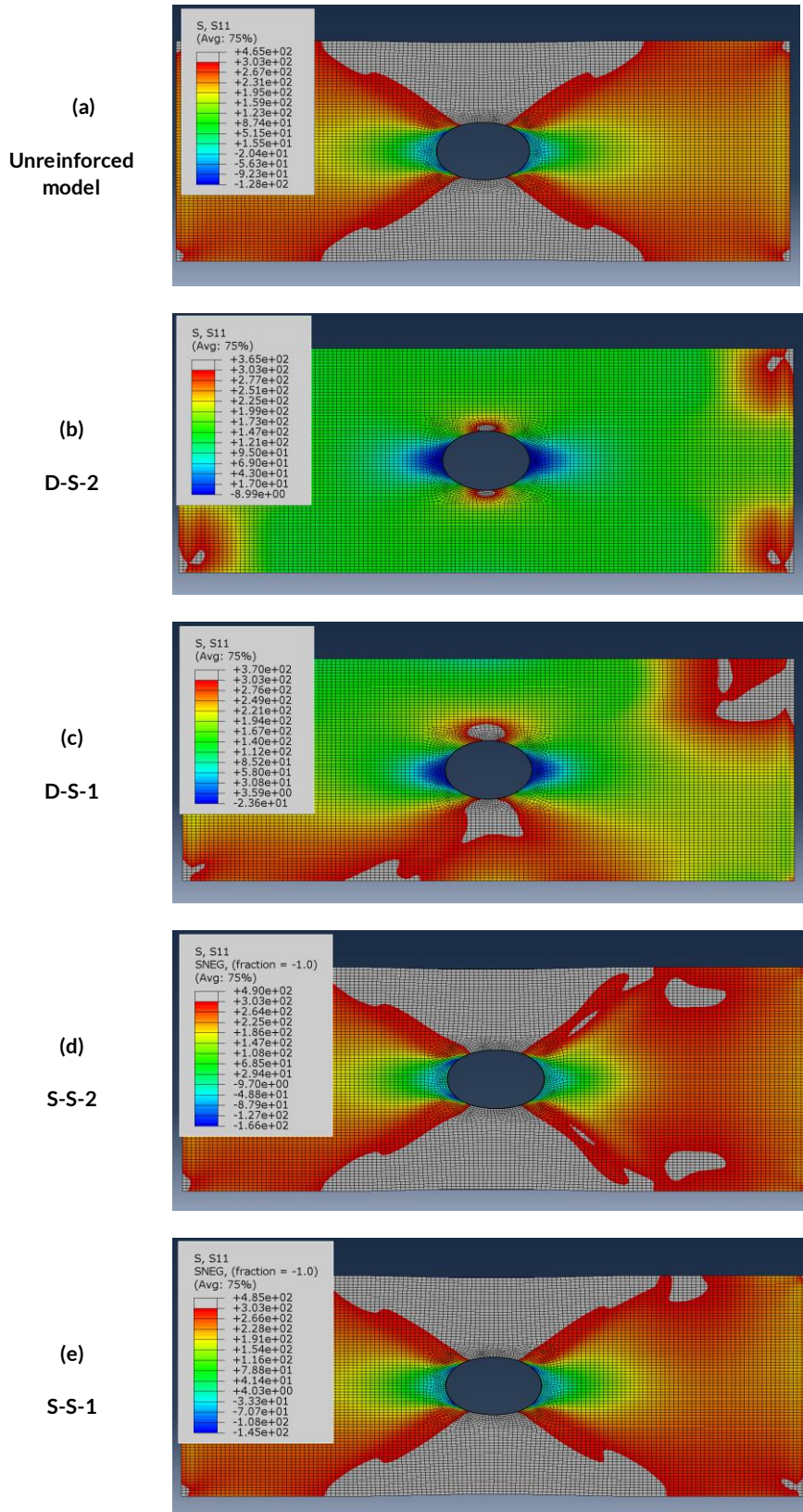


Figure 9: Contour plot of the principal stress S11 in the loading direction.

**4.2 Stiffness degradation and failure of the cohesive zone elements**

In this section, the damage state of the cohesive elements for the four reinforced models is presented. Figure (10) shows the level of stiffness degradation presented in terms of a ratio “SDEG” that is equal to 0 when the cohesive element do not experience any degradation, and equal to 1 when complete failure of the element occurs. Figure (10-a) presents the state of the cohesive zone elements for the S-D-2 model, at 340MPa applied loading stress. As can be seen, the adhesive layer experienced considerable stiffness degradation in the edge region due to peeling stresses. A reduction of 99.5% of

stiffness can be observed. On the other hand, the remaining part of the adhesive layer did not experience any damage. Figure (10-b) shows that complete failure of the cohesive element in the edge of the adhesive layer occurred for D-S-1. The initiation of delamination was observed at an applied nominal stress of 315MPa. Propagation of damage followed as the loading increased. Similar situations can be observed in Figure (10-c) and Figure (10-d), where models with single-sided CFRP configuration experienced delamination at the cohesive zone elements. The failure in the cohesive elements initiated at an applied nominal loading stress of 286 MPa for both S-S-2 and S-S-1.

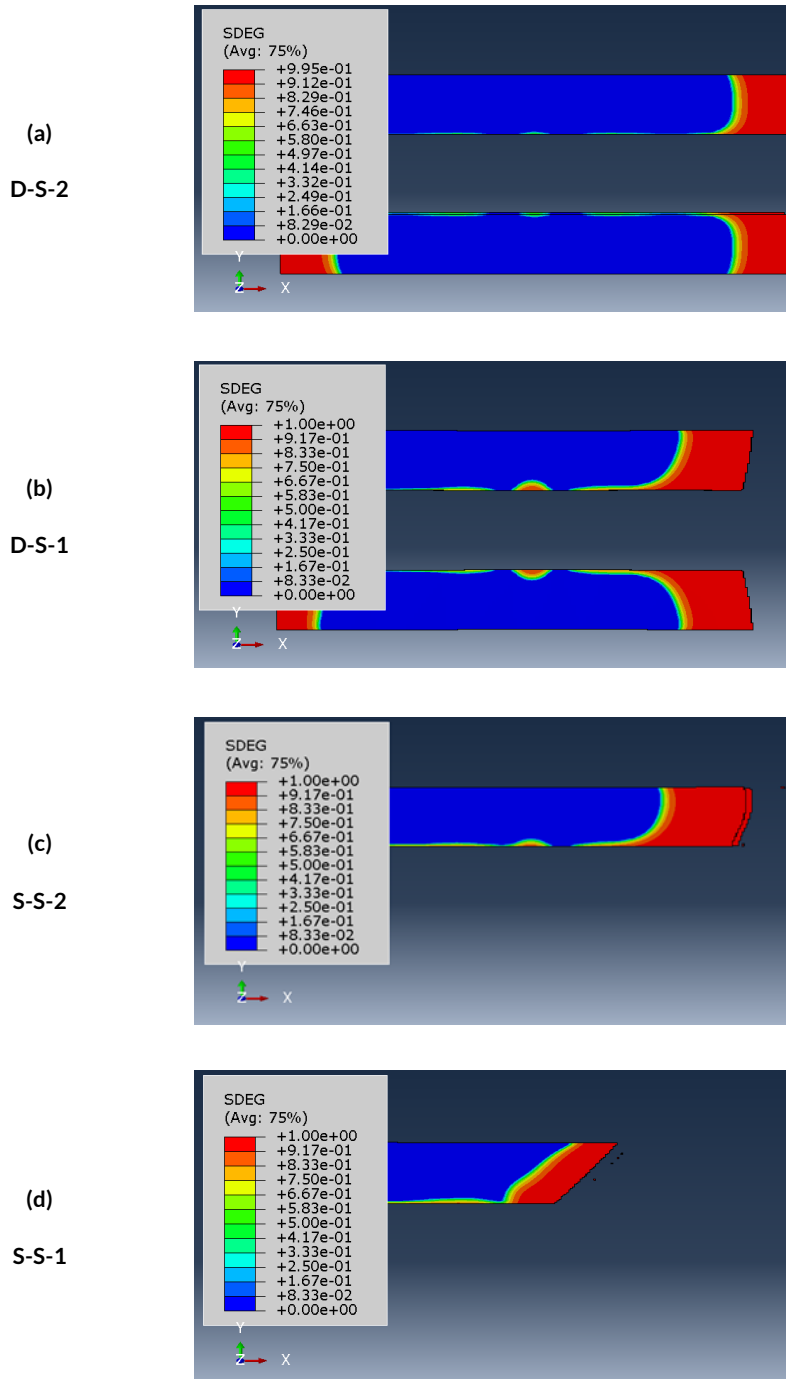


Figure 10: Stiffness degradation of the cohesive zone elements.

5 Fatigue resistance estimation

The purpose of this section is to compare the fatigue life of the unreinforced metallic plate and the ones reinforced with CFRP to investigate the efficiency of the application CFRP to extend the fatigue life of metallic components. The fatigue resistance is estimated using the local approach based on fatigue strain life. As shown in the previous section, models with single-sided CFRP configuration showed very poor performance, therefore, they are excluded from this study. So, only D-S-2 and D-S-1 are considered for fatigue life estimation.

Generally, the fatigue crack initiation arises due to plasticity at the notch root where there is a high concentration of stresses. The assessment of crack initiation using local approaches consists of assuming that the material near the notch experiences the same mechanical behavior as a smooth specimen tested under low cycle fatigue. So, the fatigue crack initiation life of a structural component can be determined by correlating the strain life of the material ( $\epsilon$ -N curve), and the elasto-plastic response obtained from the structural analysis.

In this study, the fatigue crack initiation life is estimated at the singular node of maximum stress concentration (i.e. near the circular hole). Morrow [28] relation, shown in equation (5), superposes the elastic strain amplitude with plastic strain amplitude to estimate the total strain fatigue life from low to high cycle fatigue regimes.

$$\frac{\Delta\epsilon}{2} = \frac{\Delta\epsilon_e}{2} + \frac{\Delta\epsilon_p}{2} = \frac{\sigma'_f}{E} (2N_f)^b + \epsilon'_f (2N_f)^c \tag{5}$$

Where,  $\sigma'_f$  is the fatigue strength coefficient, b is the fatigue strength exponent and E is the Young's modulus. The coefficients  $\epsilon'_f$  and c are the fatigue ductility coefficient and fatigue ductility exponent, respectively.

The parameters of the equation (5) used in this study, were calibrated by De Jesus *et al.* [20] who tested the material extracted from Luiz I Bridge under high and low cycle fatigue regimes. The experimental results were correlated with the Morrow's equation, as shown in Figure (11).

In this study, the procedure used to determine the fatigue life of the metallic plates consisted of equating Morrow's equation and the strains obtained from the numerical analysis to find the number of cycles at failure " $N_f$ ", for different applied stress levels. The solution of the mathematical equation was obtained using the Secant method algorithm. The accuracy of results provided by the numerical solver was verified. Finally, a relationship between the stress range of the applied nominal stress " $\Delta\sigma$ " and the " $N_f$ " could be obtained.

Figure (12) illustrates the fatigue resistance curves for the unreinforced metallic plate and for the reinforced plates D-S-2 and D-S-1. A logarithmic scale is adopted to establish the linear relationship between the stress range and the number of cycles to failure. The numerical results are shown in scatter points in the graph. Fatigue resistance curves are obtained using linear regression analysis. The mathematical relation is expressed by the Basquin relation, as given by equation (6)

$$\Delta\sigma^m N_f = C \tag{6}$$

Where  $\Delta\sigma$  is the nominal stress range, C and m are constants. The parameters for the three lines are presented in table (3).

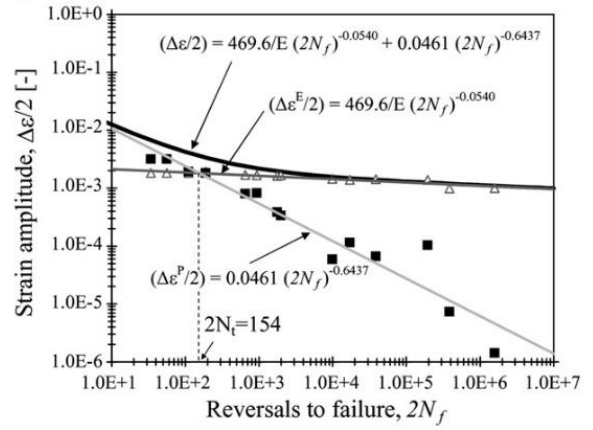


Figure 11: Strain life according to Morrow's curve for puddle iron of Luiz I Bridge, Porto, Portugal (De Jesus *et al.* [20]).

It can be seen, that the application of CFRP shifts the curve towards higher fatigue performance. D-S-2 shows a significant increase in fatigue life, where the results depict a very high value of " $N_f$ " at large applied nominal stress around 300MPa which is very close to the yield strength of the metal. D-S-1 shows also a considerable increase in fatigue life.

Therefore, it can be concluded that the application of ultra-high modulus CFRP with double-sided configuration is expected to be very efficient in increasing the fatigue life of a metallic structural component.

Table 3 Parameters of the fatigue resistance curves.

Model	m	c
Unreinforced	21.94	3.82797E+54
D-S-1	33.13	1.077409E83
D-S-2	27.662	1.4750414E76

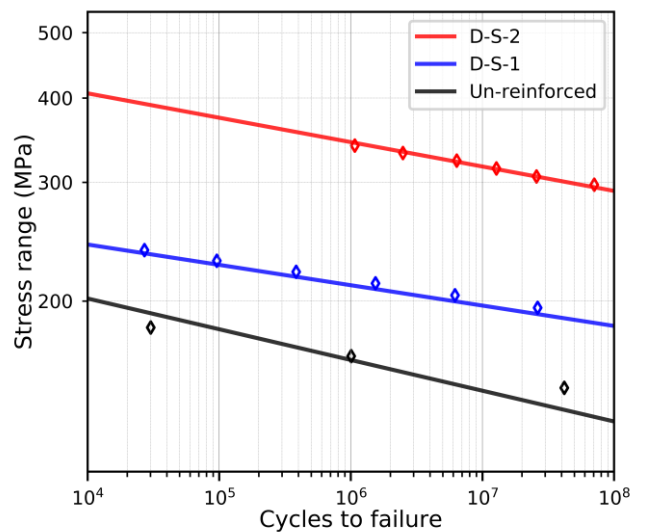


Figure 11: Fatigue resistance curves for the unreinforced and reinforced metallic plates.

## 6 Summary and discussion

This paper presents a numerical investigation on the fatigue life of non-cracked metallic small-scale specimens reinforced with CFRP. The metallic plates feature a circular hole in the center to represent the geometry of metallic splices in riveted connections, commonly found in old metallic bridges. The nonlinear mechanical behavior of the puddle iron extracted from Luiz I Bridge (Porto, Portugal) is simulated in the numerical model. The reinforcements adopted consist of using ultra-high modulus CFRP ( $E=440\text{GPa}$ ) bonded with high tensile strength epoxy. Cohesive zone modeling technique was adopted in the numerical model to simulate the full behavior of the adhesive layer including the elastic behavior, stiffness and strength degradation, as well as the initiation and propagation of the crack. The failure in the cohesive zone elements was based on an energy criterion. The cohesive zone model was calibrated using parameters derived from fracture mechanics tests on the adhesive. Four CFRP patching configurations were investigated, considering double and single-sided with two or one CFRP plates. All models were subjected to a gradual static monotonic loading up to a very high level of nominal stress with a value of  $340\text{MPa}$ .

The results of the reinforced elements were compared with an unreinforced bare metallic plate used as a reference. Double sided configurations (i.e. D-S-2 and D-S-1) showed a much better performance than single-sided ones (S-S-2 and S-S-1). Due to the asymmetry of the CFRP plates in one sided configuration, additional bending stresses were induced in the unreinforced side of the metallic plates. The level of stress raised higher than the reference model. Therefore, single-sided configuration was judged to be inefficient. Note that in this study, the stress and strains are measured at singular stress point in the concentration zone. The size effect (see refs. [29], [30]) of the stress concentration zone is beyond the scope of this study. The double-sided configuration with two CFRP plates showed the best performance. Where, the stress level near the circular hole decreased dramatically by 45%. Besides, delamination in the cohesive zone elements did not occur. Double sided configuration with one CFRP plate in each side showed a lower performance with delamination in the cohesive zone at high level of applied nominal stress (i.e.  $\sigma > 315\text{MPa}$ ).

Fatigue resistance curves for the double sided reinforced models and a bare metallic model without reinforcement were derived using local approach based on fatigue strain life of the material which was defined according to Morrow's equation in previous related study for the puddle iron of Luiz I Bridge Porto. The results show that the application of the ultra-high modulus CFRP with double sided configuration increases the fatigue life of the structural component significantly. Note that in this study, degradation of the adhesive layer due to fatigue loading is not considered. Previous experimental studies (e.g. Wu *et al.* [31]) showed that the adhesive layer is insensitive to the fatigue loading only when the level of stress in the adhesive layer is lower than 30% of the adhesive strength. Therefore, the inclusion of the strength degradation in the adhesive layer due to the fatigue loading is recommended for future studies.

### Acknowledgment

This work was financially supported by: Base Funding - UIDB/04708/2020 and Programmatic Funding - UIDP/04708/2020 of the CONSTRUCT - Instituto de I&D em Estruturas e Construções - funded by national funds through the FCT/MCTES (PIDDAC).

The authors gratefully acknowledge the funding of FiberBridge - Fatigue strengthening and assessment of railway metallic bridges using fiber-reinforced polymers (POCI-01-0145-FEDER-030103) by FEDER funds through COMPETE2020 - Programa Operacional

Competitividade e Internacionalização (POCI) and by national funds (PIDDAC) through Portuguese Science Foundation (FCT/MCTES).

### References

- [1] J. Wallin, J. Leander, and R. Karoumi, "Strengthening of a steel railway bridge and its impact on the dynamic response to passing trains," *Eng. Struct.*, vol. 33, no. 2, pp. 635–646, 2011.
- [2] A. Bassetti, P. Liechti, and A. Nussbaumer, "Fatigue resistance and repairs of riveted bridge members," *Eur. Struct. Integr. Soc.*, vol. 23, no. C, pp. 207–218, 1999.
- [3] A. Bassetti, A. Nussbaumer, and P. Colombi, "Repair of Riveted Bridge Members Damaged By fatigue using CFRP materials," in *Advanced FRP Materials for Civil Structures*, 2000, pp. 33–42.
- [4] P. Colombi, A. Bassetti, and A. Nussbaumer, "Analysis of cracked steel members reinforced by pre-stress composite patch," *Fatigue Fract. Eng. Mater. Struct.*, vol. 26, no. 1, pp. 59–66, 2003.
- [5] S. C. Jones, S. A. Civjan, and M. Asce, "Application of Fiber Reinforced Polymer Overlays to Extend Steel Fatigue Life," *J. Compos. Constr.*, vol. 7, no. November, pp. 331–338, 2003.
- [6] E. Lepretre, S. Chataigner, L. Dieng, and L. Gaillet, "Fatigue strengthening of cracked steel plates with CFRP laminates in the case of old steel material," *Constr. Build. Mater.*, vol. 174, pp. 421–432, 2018.
- [7] H. Liu, R. Al-Mahaidi, and X. L. Zhao, "Experimental study of fatigue crack growth behaviour in adhesively reinforced steel structures," *Compos. Struct.*, vol. 90, no. 1, pp. 12–20, 2009.
- [8] H. T. Wang, G. Wu, and J. B. Jiang, "Fatigue behavior of cracked steel plates strengthened with different CFRP systems and configurations," *J. Compos. Constr.*, vol. 20, no. 3, pp. 1–9, 2016.
- [9] P. Colombi, G. Fava, and L. Sonzogni, "Effect of initial damage level and patch configuration on the fatigue behaviour of reinforced steel plates," *Fatigue Fract. Eng. Mater. Struct.*, vol. 38, no. 3, pp. 368–378, 2015.
- [10] P. Colombi, G. Fava, and L. Sonzogni, "Fatigue crack growth in CFRP-strengthened steel plates," *Compos. Part B*, vol. 72, pp. 87–96, 2015.
- [11] Q. Yu and T. Chen, "Tests on Cracked Steel Plates with Different Damage Levels Strengthened by CFRP Laminates," *Int. J. Struct. Stab. Dyn.*, vol. 14, no. 6, pp. 1–26, 2014.
- [12] Q. Q. Yu, T. Chen, X. L. Gu, X. L. Zhao, and Z. G. Xiao, "Fatigue behaviour of CFRP strengthened steel plates with different degrees of damage," *Thin-Walled Struct.*, vol. 69, pp. 10–17, 2013.
- [13] N. J. Aljabar, X. L. Zhao, R. Al-Mahaidi, E. Ghafoori, M. Motavalli, and N. Powers, "Effect of crack orientation on fatigue behavior of CFRP-strengthened steel plates," *Compos. Struct.*, vol. 152, pp. 295–305, 2016.
- [14] N. J. Aljabar, X. L. Zhao, R. Al-mahaidi, E. Ghafoori, M. Motavalli, and Y. C. Koay, "Fatigue tests on UHM-CFRP strengthened steel plates with central inclined cracks under different damage levels," *Compos. Struct.*, vol. 160, pp. 995–1006, 2017.
- [15] E. Ghafoori, M. Motavalli, A. Nussbaumer, A. Herwig, G. S. Prinz, and M. Fontana, "Determination of minimum CFRP pre-stress levels for fatigue crack prevention in retrofitted metallic beams," *Eng. Struct.*, vol. 84, pp. 29–41, 2015.
- [16] E. Ghafoori and M. Motavalli, "A retrofit theory to prevent fatigue crack initiation in aging riveted bridges using carbon fiber-reinforced polymer materials," *Polymers (Basel)*, vol. 8, no. 8, 2016.

- [17] E. Ghafoori *et al.*, "A strengthening theory to prevent fatigue crack initiation in old metallic bridges," *Maintenance, Monit. Safety, Risk Resil. Bridg. Bridg. Networks - Proc. 8th Int. Conf. Bridg. Maintenance, Saf. Manag. IABMAS 2016*, no. June, 2016.
- [18] E. Ghafoori, M. Motavalli, X. L. Zhao, A. Nussbaumer, and M. Fontana, "Fatigue design criteria for strengthening metallic beams with bonded CFRP plates," *Eng. Struct.*, vol. 101, pp. 542–557, 2015.
- [19] K. A. Harries, "Editor's Note – Chock Full O' Case Studies West," in *FRP International*, 2011, vol. 8, no. 3, pp. 1–14.
- [20] A. M. De Jesus, A. L. L. d. Silva, M. V. Figueiredo, J. A. F. O. Correia, A. S. Ribeiro, and A. A. Fernandes, "Strain-life and crack propagation fatigue data from several Portuguese old metallic riveted bridges," *Eng. Fail. Anal.*, vol. 18, no. 1, pp. 148–163, 2011.
- [21] J. A. F. de O. Correia, "PhD Thesis: An Integral Probabilistic Approach for Fatigue Lifetime Prediction of Mechanical and Structural Components," 2014.
- [22] S. S. J. Moy, "CFRP strengthening of cast and wrought iron structures," in *SMAR- Fourth Conference on Smart Monitoring, Assessment and Rehabilitation of Civil Structures*, 2017.
- [23] R. D. S. G. Campilho, M. D. Banea, A. M. G. Pinto, L. F. M. Da Silva, and A. M. P. De Jesus, "Strength prediction of single- and double-lap joints by standard and extended finite element modelling," *Int. J. Adhes. Adhes.*, vol. 31, no. 5, pp. 363–372, 2011.
- [24] R. HAGHANI, *Rehabilitation of Metallic Civil Infrastructure Using Fiber Reinforced Polymer (FRP) Composites: Types Properties and Testing Methods*, Chalmers U. Sweden, 2014.
- [25] A. Turon, C. G. Dávila, P. P. Camanho, and J. Costa, "An engineering solution for mesh size effects in the simulation of delamination using cohesive zone models," *Eng. Fract. Mech.*, vol. 74, no. 10, pp. 1665–1682, 2007.
- [26] K. Song, C. Davila, and C. Rose, "Guidelines and parameter selection for the simulation of progressive delamination," *2008 ABAQUS User's Conf.*, pp. 1–15, 2008.
- [27] S. Fawzia, X. L. Zhao, and S. Rizkalla, "BOND CHARACTERISTICS BETWEEN CFRP AND STEEL PLATES IN DOUBLE STRAP JOINTS," *J. Adv. steel Constr.*, vol. 1, no. 2, pp. 17–27, 2005.
- [28] J. Morrow, "Cyclic Plastic Strain Energy and Fatigue of Metals," *Intern. Frict. Damping, Cycl. Plast. ASTM Int.*, pp. 45–87, 1965.
- [29] M. Muniz-Calvente, A. M. P. de Jesus, J. A. F. O. Correia, and A. Fernández-Canteli, "A methodology for probabilistic prediction of fatigue crack initiation taking into account the scale effect," *Eng. Fract. Mech.*, vol. 185, pp. 101–113, 2017.
- [30] Y. Ai, S. P. Zhu, D. Liao, J. A. F. O. Correia, A. M. P. De Jesus, and B. Keshtegar, "Probabilistic modelling of notch fatigue and size effect of components using highly stressed volume approach," *Int. J. Fatigue*, vol. 127, no. April, pp. 110–119, 2019.
- [31] C. Wu, X. L. Zhao, W. K. Chiu, R. Al-Mahaidi, and W. H. Duan, "Effect of fatigue loading on the bond behaviour between UHM CFRP plates and steel plates," *Compos. Part B Eng.*, vol. 50, pp. 344–353, 2013.